Encapsulation of Ar_n complexes by Calix[4]arene: *Endo*- vs. *exo*-complexes

Takayuki Ebata[1*], Naoya Hontama[1], Yoshiya Inokuchi[1], Takeharu Haino[1]

Edoardo Aprà[2] and Sotiris S. Xantheas[3*]

[1] Department of Chemistry, Graduate School of Science, Hiroshima University, Higashi-Hiroshima 739-8526, Japan

[2] Computer Science and Mathematics Division, Oak Ridge National Laboratory, Oak Ridge, TN 37831, USA

[3] Chemical & Materials Sciences Division, Pacific Northwest National Laboratory, 906 Battelle Boulevard, P.O. Box 999, MS K1-83, Richland, WA 99352, USA

Abstract

The structure of the calix[4]arene(C4A)-Ar_n complexes has been investigated by laser induced fluorescence spectroscopy, mass-selected resonant two-color two-photon ionization (2C-R2PI) spectroscopy, fragment detected IR photodissociation (FDIRPD) spectroscopy, and high level first principles electronic structure calculations at the MP2 and CCSD(T) levels of theory. C4A has a very high ability of forming van der Waals complexes with rare gas atoms. For the C4A-Ar dimer, two isomers are found. A major species shows a 45 cm^{-1} red-shift of its band origin with respect to the monomer, while that of a minor species is 60 cm^{-1}. The binding energy the major species is determined to be in the range of 350 - 2250 cm^{-1} from 2C-R2PI spectroscopy and FDIRPD spectroscopy. Two isomers are also identified in the quantum chemical calculation, depending on whether the Ar atom resides inside (*endo*) or outside (*exo*) the C4A. We propose a novel scheme to derive CCSD(T)-quality binding energies for the C4A-Ar complex based on the ratio of CCSD(T)/MP2 energies for the smaller model systems Benzene-Ar and Phenol-Ar. Our best computed estimates for the binding energies of the C4A-Ar *endo*- and *endo*-complexes are 1560 cm^{-1} and 510 cm^{-1}, respectively, at the CCSD(T)/Complete Basis Set (CBS) level of theory. For the C4A-Ar_2 trimer, we again identified two isomers in the calculation: one is the {2:0} *endo*-complex in which the Ar_2 dimer is encapsulated inside the C4A cavity and the other is the {1:1} *endo-exo*-complex in which one Ar resides inside and the other outside the C4A cavity. The calculated binding energies for the two C4A-Ar_2 isomers are nearly identical. However, the experimental evidence strongly suggests that the observed species is the

{2:0} *endo*-complex. The *endo* structural motif is also suggested for the larger C4A-Ar_n complexes because of the systematic red-shifts of the complexes with the number of bound Ar atoms, that is the Ar_n complex is encapsulated inside the C4A cavity. The formation of the *endo*-complex structures is attributed to the anisotropy of the interaction with C4A during the complex formation in the expansion region.

1. Introduction

Calixarenes (CAs) are cyclic oligomers built with phenol units and act as molecular receptors that form a variety of complexes with metal ions, anions and neutral molecules.[1-3] The structural motif of CAs consists of a cavity demarcated by benzene rings and the presence of multiple hydroxyl groups in the lower rim of that cavity that form strong homodromic intramolecular hydrogen bonds. This strong intramolecular H-bonding leads to pKa values for CAs being different from the monomeric units,[4,5] and the balance of the interaction between the guest molecule and either the benzene or the hydroxyl group site is very subtle. For example, recent studies reported that the "Calix[4]arene(C4A) - aliphatic amine" complex exists as the *exo*-complex in which a protonated amine is bound to C4A outside the cavity via the N^+–H---O^- form,[6,7] though the complex was initially suggested to be the *endo*-complex. The complexation structures of CAs have been studied by NMR and X-ray diffraction methods in the condensed phase,[8-11] and mass spectrometric characterization combined with electrospray ionization (ESI) has been used to characterize the gas phase structures.[12,13] They have been mostly carried out at room temperature. Since the thermal energy at these temperatures is oftentimes comparable with the host-guest interaction energy, one may obtain the information averaged over all possible conformers at a given temperature. One of the methods to solve this problem and to study a specific species in detail is to use the supersonic expansion technique. By reducing the internal temperature as well as the number of isomers, we can measure the electronic and vibrational spectra of a well-specified complex and obtain the structure

of the complex unambiguously with an aid of quantum chemical calculation. Very recently, we reported laser spectroscopic and theoretical study on the structure of C4A-H_2O complex formed in a supersonic beam.[14] The structure was initially expected to be the *exo*-complex from the analogy of the condensed phase. However, it turned out that the most stable structure was the *endo*-complex in which a water molecule resides inside the C4A cavity and the complex is stabilized by the OH-π hydrogen bonding and the dipole-dipole interaction. This study demonstrated that the combination of the supersonic beam and laser spectroscopy provides us with a new tool to study the encapsulation structure of functional molecules with an aid of quantum chemical calculation.

In the present study, we report a study of the structure of the C4A-Rg van der Waals complexes. Here Rg refers a rare gas atom, but we mostly concentrate on Ar atom. Contrary to the extensive studies of the host-guest complex formation between CAs and hydrophilic molecules through CH-π interactions, little is known about the complex formation with molecular or atomic species through pure van der Waals interaction. The most interesting aspect of the CA-Rg *endo*-complex is the binding energy of the Rg atom to the cavity. Since the Rg atom is attracted by multiple phenyl groups, this results in a large binding energy and a high affinity for encapsulation compared to normal van der Waals complexes of Rg atoms with aromatic molecules. In addition, this composite interaction will be an important factor on the structure for larger size CA-$(Rg)_n$ complexes. In a previous study we reported a laser spectroscopic study on the van der Waals complexes between C4A and Ar or Ne.[15] We proposed that

C4A-Ar(Ne) adopts the *endo*-complex structure, while for C4A-Ar(Ne)$_n$ (n>1) the Ar(Ne) atoms are located outside the cavity as suggested from the analysis of the red-shifts of the electronic transitions. However, there was no further experimental or theoretical information that supported the proposed structure, such as the binding energies of the various C4A-Ar isomers.

In this study we report a joint experimental (spectroscopic) - theoretical (first principles quantum chemical) study aimed at revisiting the structure of C4A-Ar$_n$ complexes. In particular, we attempt to address the following questions:

(1) What are the theoretical requirements needed to accurately describe those weak interactions and consequently how can we arrive at accurate estimates for the binding energies of the C4A-Ar *endo*- and *exo*-complexes?

(2) Can we detect the two isomers of C4A-Ar, *endo*- and *exo*-complexes, experimentally?

(3) Which is the most stable structure of the C4A-Ar$_2$ complex and what is the energy separation between the {2:0} (Ar$_2$ is encapsulated inside the cavity) and {1:1} isomers (one Ar atom is inside and the other outside the cavity)? How large is the energy separation between them?

(4) What are the structures of the larger C4A-(Ar)$_n$ complexes for n>2?

In order to address those questions, we have relied on a combination of spectroscopic measurements and high-level electronic structure calculations that push the current state-of-the-art in the field. In particular, we measured the mass-selected resonant two-color two-photon ionization (2C-R2PI) spectra in order to (*i*) identify the

complexes, (*ii*) determine the ionization potential and (*iii*) obtain the $[C4A\text{-}Ar]^+ \rightarrow C4A^+ + Ar$ dissociation energy. In addition, we observed the IR photodissociation spectrum of the $C4A\text{-}Ar_1$ complex to obtain the $C4A\text{-}Ar_1 \rightarrow C4A + Ar$ dissociation energy. The experimental results are compared with high level electronic structure calculations for the structures and energetics of the $C4A\text{-}Ar_n$, n=1, 2 complexes, which are benchmarked against the results for smaller planar aromatic molecule – Ar systems, such as Benzene-Ar and Phenol-Ar. Based on those results we discuss the most probable structures of the larger $C4A\text{-}Ar_n$ complexes.

2. Experimental techniques

In the present work we obtained the mass-resolved two-color resonance two-photon ionization (2C-R2PI) of the $C4A\text{-}Rg_1$ complex. In particular, the 2C-R2PI technique was applied to $C4A\text{-}Ar_1$ in order to obtain the $[C4A\text{-}Ar_1]^+ \rightarrow C4A^+ + Ar$ dissociation energy, which can, in turn, be used to estimate the dissociation energy of the neutral species. In addition, we observed the fragment detected IR photodissociation (FDIRPD) spectrum of $C4A\text{-}Ar_1$ in order to obtain its dissociation energy directly. The schemes of FDIRPD spectroscopy was described in our previous paper.[14] Briefly, a tunable IR light, ν_{IR}, excites the IR band of C4A-Ar. This IR excitation depletes the population of the ground state. Thus, by scanning the IR laser frequency while monitoring the ground state population by R2PI, we obtain the IR-UV dip spectrum. When the IR photon energy is larger than the dissociation energy of C4A-Ar, the complex then dissociates to C4A and Ar, and the C4A fragment is monitored by R2PI

with the UV laser light, ν_{UV}. By scanning the IR frequency while monitoring the C4A fragment we obtain the FDIRPD spectrum. By comparing the IR-UV double resonance spectrum, we can obtain the dissociation energy.

Jet-cooled C4A and its van der Waals complexes with Rg were generated by an adiabatic expansion of the sample vapor diluted with Rg/Ne mixed carrier gas at a total pressure of 2 bar. Since C4A is a nonvolatile molecule, a high temperature pulsed nozzle, described in a previous paper, was used.[16] The gaseous C4A was expanded into vacuum through the nozzle with a 1mm orifice. The supersonic jet was subsequently skimmed by a skimmer with 2 mm aperture, located at 50 mm downstream from the nozzle. The C4A-$(Rg)_n$ complex in the supersonic beam crossed the UV laser and was ionized by R2PI. The ions were extracted into a time-of-flight (TOF) tube, and were detected by a Channeltron (Burle 4900) detector. The TOF profile was monitored by a digital oscilloscope, and the ion signals were processed by a boxcar integrator (Stanford research systems SR245) connected to a personal computer. The tunable UV laser was a second harmonic (Inrad Auto-tracker III/BBO crystal) of Nd:YAG laser pumped dye laser (Continuum Surelite II/Lambda Physique Scanmate). For 2C-R2PI experiment, either the second harmonic of another Nd:YAG laser pumped dye laser (Continuum Surelite II/ND 6000) or the third harmonic of the Nd:YAG laser was used for the ionization step. The delay time between the first laser and the second laser was fixed to several nanoseconds. IR-UV dip spectroscopy was described in previous papers. [14-16] For obtaining the FDIRPD spectrum, the frequency of the UV probe laser is fixed to a few wavenumber lower frequency position of the 0,0 band of C4A to detect the C4A

fragment, and the frequency of a tunable IR laser (Laser Vision/Quanta-Ray, GCR250) light, introduced coaxially to the UV probe laser 110 ns prior to the probe pulse, was scanned to vibrationally excite C4A-Ar complex. C4A (98%) was purchased from the Tokyo Chemical Industry Co. and was used without further purification. For the FDIRPD measurement we synthesized C4A-d_n (the H atoms in the OH groups were exchanged by D atoms), in order to probe the H-bonded OD stretching vibrations located at 2200-2400 cm^{-1}, the lowest frequency range that can be accessed with our OPO system. The H/D isotope exchange reaction of the entire phenolic hydrogens on the C4A lower rim was carried out in methanol-d_4. A suspension of the C4A in methanol-d_4 was stirred at 40°C for a few hours and the solvent was then removed *in vacuo*. The completion of the exchange reaction was confirmed by the disappearance of the ^{1}H NMR signal attributed to the phenolic hydrogens. The resultant solution was used without further purification.

3. Computational methods

3.1. Strategy

Given the nature of the interactions between the "host" C4A cavity and the "guest" Ar atom, higher levels of electron correlation and large basis sets of diffuse character are needed in order to arrive at a converged value for the [redacted] interaction energy. The size of the host cavity (C4A: 56 atoms, 224 electrons) currently prohibits the use of very large basis sets in conjunction with higher levels of electron correlation. To this end, the following computational strategy was adopted: the

binding energies of Ar with benzene and phenol (which are the building blocks of C4A) were first obtained at the second order Moller-Plesset (MP2)[17] and coupled-cluster singles and doubles with perturbative estimate of triple excitations [CCSD(T)] levels of theory[18,19] with the family of augmented correlation consistent basis sets of Dunning and co-workers[20,21] up to quadruple-zeta quality (aug-cc-pV*n*Z, *n* = D, T, Q). In this manner the effect of higher electron correlation (measured by the difference between the MP2 and the CCSD(T) results) as well as that of the basis set (difference between the aug-cc-pVDZ and aug-cc-pVQZ results) for both the MP2 and CCSD(T) levels of theory was assessed. For the C4A-Ar complex, the currently highest possible calculations were performed and – assuming a qualitatively similar behavior of the C4A-Ar energetics with those for the smaller benzene-Ar (Bz-Ar) and phenol-Ar (Ph-Ar) systems – accurate estimates at the CCSD(T) / Complete Basis Set (CBS) limit for the binding energy of the C4A-Ar system were obtained. The CCSD(T)/aug-cc-pVDZ results presented in this study currently push the limit for the state-of-the-art in the field of highly correlated electronic structure calculations.

3.2. Details of the calculations

The geometries of the benzene-Ar (Bz-Ar) and phenol-Ar (Ph-Ar) complexes were optimized at the MP2/aug-cc-pVDZ level of theory and those geometries were used for single point calculations with the larger basis sets up to the aug-cc-pVQZ at the MP2 and CCSD(T) levels of theory. The geometries of the *endo*- and *exo*-isomers of the C4A-Ar complex were also optimized at the MP2/aug-cc-pVDZ level of theory and

those geometries were used to perform single point MP2 calculations with the aug-cc-pVTZ and aug-cc-pVQZ sets and a single point CCSD(T)/aug-cc-pVDZ calculation. The use of the MP2/aug-cc-pVDZ geometries in the larger calculations for the Bz-Ar and Ph-Ar dimers was dictated from the need to adopt the same procedure for the C4A-Ar complex, for which optimizations with the larger aug-cc-pVTZ are not currently practical.

The binding energies of the various C4A-Ar dimers are computed as:

(1)

where superscripts denote basis sets and subscripts indicate the geometries of the individual species identified in parentheses. In this notation, for example, denotes the energy of C4A at the dimer (C4A-Ar) geometry with the monomer (C4A) basis set.

The basis set superposition error (BSSE) correction was estimated via the function counterpoise (fCP) method[22] including the fragment relaxation terms,[23] which arise from the change in the intramolecular geometry of C4A in the complex minimum. The BSSE-corrected dimer binding energies are:

(2)

and

. (3)

A total of 2 (since the second fragment is an atom and therefore and) additional calculations (C4A

with the full complex basis at the complex and isolated MP2/aug-cc-pVDZ geometries) are therefore required for each BSSE calculation.

The estimation of the Complete Basis Set (CBS) limit for the binding energies of the Bz-Ar and Ph-Ar complexes was performed by monitoring the *average* of the uncorrected and BSSE-corrected binding energies from equations (1) and (2) rather than applying any of the previously introduced heuristic extrapolation schemes.[24,25] For the Bz-Ar and Ph-Ar systems the ratio of the CCSD(T)/MP2 binding energies for each basis set was also computed. The ratio of the for the smaller (Bz-Ar and Ph-Ar) systems was compared to the one computed for the C4A-Ar complex with the aug-cc-pVDZ basis set and it was used to obtain the CCSD(T)/CBS estimates from the MP2 binding energies of the C4A-Ar complex with the larger basis sets. Previous calculations[26] as well as our current results for Bz-Ar and Ph-Ar suggest that electron correlation beyond MP2 is needed in order to obtain quantitative binding energies for those weakly interacting systems. To this end one might suggest that an MP2/aug-cc-pVQZ calculation for C4A-Ar is not justified since the method itself (MP2) will not converge to the correct limit for a large basis set. However, as it will be shown in the Results section (*vide infra*), this large MP2 calculation is useful since the ratio of the CCSD(T)/MP2 binding energies for the smaller Bz-Ar and Ph-Ar systems is the same with the one for the larger C4A-Ar system and therefore can be used to estimate the CCSD(T)/CBS binding energy for that complex.

The largest calculations performed in this study for the C4A-Ar complex (57 atoms, 242 electrons, C_4 symmetry for the *endo*- but C_1 symmetry for the *exo*-complex)

were single point calculations with the aug-cc-pVQZ basis set at the MP2 level (3,748 basis functions, up to 2 *g* functions per heavy atom) and with the aug-cc-pVDZ basis set at the CCSD(T) level (979 basis functions, up to 2 *d* functions per heavy atom). All calculations for the Bz-Ar and Ph-Ar systems and the MP2 calculations for the C4A-Ar complex were run on "Chinook", a 160 TFlops system consisting of 2310 HP DL185 nodes with dual socket, 64-bit, Quad-core AMD 2.2 GHz Opteron processors (Barcelona) at the Environmental Molecular Sciences Laboratory (EMSL).[27] The CCSD(T)/aug-cc-pVDZ calculations for the C4A-Ar complex were run on the CRAY XT5 partition at the ORNL Leadership Computing Facility. The ORNL XT5 partition contains 18,688 compute nodes, each made of two quad-core AMD Opteron (Barcelona) processors at 2.3 GHz, 16GB of memory, and a SeaStar 2+ network router (with a peak bandwidth of 57.6GB/s). The resulting partition contains 149,504 processing cores, resulting in more than 300 TB of memory, and a peak double precision floating-point performance of 1.38 petaFlop/s. The calculations were made possible using a modified version of the NWChem 5.1 release.[28] Modifications were introduced both in the Fortran source code of the CCSD(T) code and in the Global Array/ARMCI layer[29] used by NWChem for parallelization. As a result of these software development modifications, the CCSD(T) code in the NWChem is capable of scaling up in excess of 230,000 processors[30] ; however, the average number of processors needed for the CCSD(T) calculations reported is this study was around 40,000.

4. Results

4.1 Electronic and time-of flight mass spectra of the C4A-Ar_n complexes

The LIF spectra of C4A at various Ar partial pressures are shown in Figure 1(a), together with the 2C-R2PI spectra with the monitored masses $[C4A]^+$ (Figure 1(b)) and $[C4A\text{-}Ar_1]^+$ (Figure 1(c)). The 0,0 band of the bare C4A is located at 35,357 cm^{-1} and that of C4A-Ar (band A) emerges at 35,312 cm^{-1}, resulting in a red-shift of 45 cm^{-1}. With an increase of the Ar partial pressure, new bands (labeled B, C, D and E) appear at the lower frequency region. They are assigned to the band origins of the larger C4A-$(Ar)_n$, n=2-5 complexes and their frequencies are listed in Table I. Also listed in that Table are the frequencies for the C4A-Ne_n complexes. As noted earlier, for C4A-Ar_1 the red shift is 45 cm^{-1}, while the additional red-shifts for the larger complexes are smaller and gradually decrease with the number of the Ar atoms. In our previous paper we suggested that the structure of the C4A-Ar complex corresponds to the *endo*-isomer, while additional Ar atoms may be located outside the C4A cavity for the larger C4A-$(Ar)_n$, n>1 complexes.[15] This was based on the observation that the ratio of the red-shift between the C4A-Ar and C4A-$(Ar)_2$ complexes is close to 4:1, a value that resembles the ratio of the phenyl rings that the Ar atom interacts with at the *endo*- and the *exo*-complex geometries. However, as it will be discussed later, the red-shift of 11 cm^{-1} for C4A-$(Ar)_2$ with respect to C4A-Ar is too small when compared to corresponding shifts for other aromatic systems with Ar atoms located in the opposite side of the aromatic ring.

In Figures 1(b) and (c), we recognize a new band A' (35,297 cm^{-1}) located

between bands B and C. Actually, this band is also identified in the LIF spectra at low Ar partial pressure. In this time-of-flight mass-spectrometry measurement (right side of Figure 1), the energy of the ionization laser, the third harmonics (355 nm) of the Nd:YAG laser, is higher than the dissociation thresholds for the processes $[C4A\text{-}Ar_1]^+ \rightarrow C4A^+ + Ar$ and $[C4A\text{-}Ar_2]^+ \rightarrow [C4A\text{-}Ar_1]^+ + Ar$ so that a large amount of the $C4A^+$ and $[C4A\text{-}Ar]^+$ fragment ions are generated for bands A and B, respectively. However, an important feature is seen in the time-of-flight spectra, namely that the $[C4A\text{-}Ar]^+/ C4A^+$ intensity ratio for bands A (0.25) and A' (0.22) is almost 1, indicating that these are very similar with each other. On the other hand, the ratio of band B (1.3) is much larger since this species is assigned to $C4A\text{-}Ar_2$. Therefore the small values and the similarity of the ratios of the bands A and A' suggests that they can be assigned to different isomers of the C4A-Ar complex.

4.2 The ionization potential of C4A and the C4A-Ar dissociation energy estimated from the mass-resolved 2C-R2PI measurements

We first tried to measure the C4A-Ar dissociation energy by the 2C-R2PI measurement . Left side of Figure 2 shows the 2C-R2PI spectra for the bare (a) C4A and (b) C4A-Ar complex. In these measurements, the first laser (ν_1) is fixed at the 0,0 band of each species and the frequency of the ionization laser (ν_2) is scanned across the ionization potential and the dissociation threshold for the complex cation. The ion intensities are plotted against the total energy ($\nu_1 + \nu_2$). The right side of Figure 2 shows the energy level diagram used to obtain the ionization potential and the binding energy

of the cationic and neutral complexes. From the 2C-R2PI spectra of the bare C4A (Figure 2(a)), we obtain the ionization potential of C4A at 62,650 cm^{-1} (7.767 eV). However, it should be noted that the spectrum does not exhibit a sharp step-like structure at IP_0 as normally expected for the bare molecule. The reason of the lack of the step structure is ascribed to the large difference in the intramolecular [redacted] equilibrium structure between the S_1 and the ionic states. A drasric decrease of the [redacted] intermolecular bond length upon the ionization is reported in many hydrogen-bonded complexes of phenol derivatives, where B refers to base. In case of C4A, a similar decrease of the intramolecular [redacted] hydrogen-bonding will occur, and we cannot access the pontential minimum of the cation due to the poor Franck-Condon overlap between the S_1 and the ioninc states. Thus, the obtained ionization potenital corresponds to an upper limit.

The lack of a accurate value for IP_0 presents a hurdle for obtaining an accurate estimate for the [redacted] binding energy. The 2C-R2PI spectrum of the C4A-Ar complex obtained by monitoring the $[C4A\text{-}Ar_1]^+$ yields an ionization potential of 62620 cm^{-1}, which is only 30 cm^{-1} less than that of the bare C4A. However, the decrease of the ionization potential by the formation of a van der Waals complex is much larger for a typical aromatic molecule. For example, the ionization potential of fluorobenzene-Ar (FB-Ar) is 222 cm^{-1} lower than that of the bare FB.[31,32] The [redacted] binding energy obtained from the appearance curve of $[C4A]^+$ fragment, Figure 2(c), using the energy level diagram in the right is 380 cm^{-1}. This binding energy is also less than the [redacted] binding energy of 543 cm^{-1}.

Since the Ar atom interacts with four phenyl rings in the C4A-Ar complex, the [redacted] binding energy should in principle be larger than that of [redacted]. Therefore from the 2C-R2PI measurement and the use of the energy diagram of Figure 2 we obtained a lower limit of 350 cm^{-1} for the [redacted] binding energy.

4.3 The C4A-Ar dissociation energy estimated from the fragment-detected IR photodissociation measurement in S_0

Another method to obtain the C4A-Ar binding energy is the IR photodissociation experiment. As was described in the experimental section, we performed this experiment for the H/D isotope exchanged C4A. Figures 3(a),(b) and (c) shows the LIF spectra of C4A, C4A-d_n , and C4A-d_n-Ar in the 0,0 band region. An appearance of several peaks in figures 3(b) and (c) is due the coexistence of several deuterated species, C4A-$d_{0,1,2,3}$. Thus, in the present experiment, we measured the IR phtotodissociation spectra for the mixed species for C4A-d_n-Ar. Even it is the case, we can safely assume that the C4A-Ar binding energy is almost the same among the isotopomers, because the C4A-Ar interaction is between Ar and the phenyl rings, and this situation is common for all the spcecies. Figure 3(d) shows the C4A fragment detected IR photodissoication (FDIRPD) spectra of C4A-d_0-Ar. In this experiment, the frequency of the monitoring laser is fixed at 35355 cm^{-1}, which is 2 cm^{-1} lower than the band origin. In the figure, a broad H-bonded OH stretching band with the peak intensity at 3260 cm^{-1} appears widely, indicating the C4A-Ar binding energy is less than this

energy region as was expected. Upper pannel of Figure 3(e) shows the FDIRPD spectrum of C4A-$d_{1,2,3}$-Ar. Since the band consists of several isotopic species, the spectrum shows complicated structure. So, we simulated IR spectrum of the OD stretching vibration by adding the bands of the C4A-$d_{1,2,3}$ isotopic species with the relative ratio observed in the LIF spectrum. For C4A-d_2, we considered two species depending on the relative position of two OD groups, that is either they are located in opposite side or in the next neighbour. The simulated IR spectrum is shown in the lower pannel of figure 3(e), which shows a good agreement with the observed spectrum. An exception is the band at 2260 cm^{-1} in figure 3(d). This band is assigned to the overtone band of the bending vibraiton of the OD groups. Since the C4A fragement is still observed even in this energy region, we conclude the upper valueof the C4A-Ar binding energy to be 2253 cm^{-1}(lower edge of this band). Finally the experimentally estimated ☐ binding energy is in the range between 350 and 2250 cm^{-1}.

4.4 Optimal structures and the binding energies of the C4A-Ar$_n$ (n=1, 2) complexes

The Bz-Ar and Ph-Ar model systems: We first investigated the effects of electron correlation and orbital basis set on the binding energies of the Bz-Ar and Ph-Ar systems, which mimic a piece of the total interaction in the C4A-Ar complex. The calculated binding energies (D_e) for those two systems are shown in Table 2 at the MP2 and CCSD(T) levels of theory with the aug-cc-pVnZ, n=D, T, Q basis sets. Zero-point energy corrected energies (D_0) include harmonic estimates of the *differences* in zero-point energies between Bz-Ar (Ph-Ar) and Bz (Ph) of 59.0 cm^{-1} (59.6 cm^{-1})

obtained at the MP2/aug-cc-pVDZ level of theory.

As noted in several earlier studies, MP2 as a method overestimates these weak interactions. Indeed, for Bz-Ar the average of the uncorrected and BSSE-corrected binding energies at the MP2/aug-cc-pVQZ level is 587 cm^{-1} (cf. Table 2), a value that is close to the MP2/CBS estimate[33] of 553 cm^{-1} previously reported at the MP2-R12 level of theory with basis sets as large as aug-cc-pV5Z. The resulting D_0=528 cm^{-1} at the MP2/aug-cc-pVQZ level is over 200 cm^{-1} larger than the experimentally obtained value[34] of 314 ± 7 cm^{-1}. Similarly, for Ph-Ar the average of uncorrected and BSSE-corrected MP2/aug-cc-pVQZ D_e's is 613 cm^{-1}, producing D_0=553 cm^{-1}, whcih is also ~200 cm^{-1} larger than the experimentally measured value[35-37] of 359 cm^{-1}.

In contrast, the CCSD(T) level of theory produces accurate binding energies for the two model systems as long as large basis sets are used. Our best-computed estimates (cf. Table 2) for D_0 are 329 cm^{-1} (Bz-Ar) and 351 cm^{-1} based on the "average" between the uncorrected and BSSE-corrected CCSD(T)/aug-cc-pVQZ energies. These are 15 cm^{-1} and 8 cm^{-1} shy of the experimentally determined values for the two systems, respectively. The ratio of the CCSD(T)/MP2 binding energies for the Bz-Ar and Ph-Ar complexes is listed in Table 3. We note that this ratio (expressed as a percentage of the CCSD(T) binding energy with respect to MP2) remains remarkably constant with basis set size for the average of the uncorrected and BSSE-corrected binding energies. For Bz-Ar the range of this ratio is < 4 percentage units for all three basis sets whereas for Ph-Ar it is smaller (< 2 percentage units).

The requirement for the use of a large basis set in conjunction with a highly

correlated method presents a problem for the accurate estimation of the binding energy of the C4A-Ar complex since CCSD(T) calculations with just the smaller aug-cc-pVDZ basis set are currently feasible. However, the finding that the ratio of CCSD(T)/MP2 binding energies lies within a very narrow range suggests that the estimation of CCSD(T)-quality binding energies for C4A-Ar from the MP2 ones can be a viable alternative, provided that the corresponding ratio for that system is roughly the same as for the smaller ones.

The *endo*- and *exo*-isomers of the C4A-Ar complex**:** The optimal MP2/aug-cc-pVDZ structures for the C4A-Ar complex are shown in figures 4(a) and (b) and their binding energies are listed in Table 4. One is the (a) *endo*-isomer in which Ar atom is loated insided the cavity along the C_4 axis, and the other is the (b) *exo*-isomer in which the Ar atom is located outside and bound to one on the phenyl ring. We note that the *endo*- is more stable than the *exo*-isomer, a result also previously found[14] for the C4A-H_2O complex (albeit for the *exo*-isomer in that case the water molecule forms a hydrogen bond with the OH groups in the lower rim of the C4A cavity instead of interacting with the aromatic ring). The best computed binding energy at the MP2/aug-cc-pVQZ level (2328 cm^{-1}) is just outside the high end of the experimental range obtained in section 4.1, a fact that is consistent with the expected overestimation of the interaction at that level of theory.

The CCSD(T)/aug-cc-pVDZ binding energgies for the *endo*-isomer are 2467 cm^{-1} (uncorrected), 1013 cm^{-1} (BSSE-corrected) and 1740 cm^{-1} (average of the previous two). This already represents a 30 % reduction from the corresponding MP2 results with

the same basis set. The CCSD(T)/MP2 ratios of binding energies computed with the aug-cc-pVDZ basis set are 78.7 % (uncorrected), 58.5% (BSSE-corrected) and 71.5 % (average of the previous two). These ratios are within 4 percentage units from the corresponding ones for the Ph-Ar system. The use of the ratios obtained for the Ph-Ar system (from Table 3) in conjunction with the MP2/aug-cc-pVDZ binding energy for C4A-Ar yields a CCSD(T)/aug-cc-pVDZ estimate (shown in italics in parentheses in Table 4) that is within 100 cm^{-1} (~6%) or less from the computed one. Our best estimates for the binding energy of the C4A-Ar complex at the CCSD(T) level are 1561 cm^{-1} (using the Ph-Ar CCSD(T)/MP2 aug-cc-pVQZ ratio and the MP2/aug-cc-pVQZ result) and 1,665 cm^{-1} (using the C4A-Ar CCSD(T)/MP2 aug-cc-pVDZ ratio and the MP2/aug-cc-pVQZ result). These two estimates are within 100 cm^{-1} (or 6%) from each other, a value that can be considered as the error bar of our extrapolation scheme. The application of the first combination to the *exo*-isomer energetics yields a best estimate of 511 cm^{-1} at the CCSD(T) level; therefore the *exo*-isomer is ~1050 cm^{-1} less stable than the *endo*-isomer. It is interesting to note that at the CCSD(T) level both isomers lie within the experimentally determined range of 350-2,250 cm^{-1} for the binding energies.

From the two-color R2PI spectra, we have identified two isomers of C4A-Ar, species A and A'. Species A is the major one and exhibits a red shift of 45 cm^{-1}, and a minor species A' exhibits a red shift of 60 cm^{-1}. From the calculated binding energies, the major species can be assigned to the *endo*-isomer and the minor one to the *exo*-isomer. The values of the red shifts of both species are quite large compared to

those of other aromatic molecules. For example, the red shifts of Bz-Ar[38] and Ph-Ar[37] are 20 and 35 cm^{-1}, respectively. The large red shifts observed for C4A-Ar are due to the large polarizability of C4A and its change upon the electronic excitation.

The structures of the C4A-Ar_2 isomers: For C4A-Ar_2, we examined two isomers as shown in Figures 5(a) and (b). One is the (a) *endo*-complex or {2:0} isomer, in which Ar_2 is encapsulated in the C4A cavity. In the {2:0} isomer, one Ar atom is located along the C_4 axis and the other is tilted toward to the middle of the two phenyl ring. The other isomer is the (b) one-*endo*-one-*exo*-complex or {1:1}isomer, in which one Ar atom is encapsulated in the C4A cavity and the other Ar is bound to one of the phenyl ring outside the cavity. The MP2/aug-cc-pVDZ (uncorrected) binding energies of these two isomers (with respect to the C4A+Ar+Ar asymptote) are 4006 cm^{-1} and 4093 cm^{-1} for the {2:0} and {1:1} isomers, respectively. For calibration, the Ar-Ar interaction at that level of theory is 89 cm^{-1} (experimental D_e is 105 cm^{-1})[39]. The {1:1} isomer was therefore found to be slightly more stable than the {2:0} isomer, albeit the difference in their binding energies is quite small. It is therefore difficult to predict which of the two isomers corresponds to the observed species B. However, the magnitude of the red-shift provides us a good hint to assign the structure of species B. It is well known that an addition rule is held for the red-shifts of the {1:1} isomer of the aromatic molecule-Rg_2 complex.[37,40,41] The red-shift of Bz-$Ar_{1,2}$ is 20 and 40 cm^{-1}, respectively,[40] and that of Ph-$Ar_{1,2}$ is 35 and 69 cm^{-1}, respectively.[37,41] Thus the red-shift of the {1:1} isomer is twice of the {1:0} complex in both cases. We can apply the same addition rule for the red-shift of the C4A-Ar_2 complex. If the complex adopts the {1:1} structure, the

red-shift with respect to bare C4A will be 105 cm^{-1}, that is the sum of 45 and 60 cm^{-1}, while the red-shift of band B is 53 cm^{-1}. Band B is only 11 cm^{-1} red-shifted with respect to band A, which means that the interaction between the second Ar atom and the phenyl ring is small. Such the weak interaction can be explained if both Ar atoms are located in the same side with respect to C4A, that is the {2:0} structure (Figure 5 (b)). As seen from the optimal structure of the {2:0} isomer, the second Ar atom is elevated with respect to the center of mass of C4A when compared to the first one and this further justifies its weaker interaction with the phenyl ring when compared to the first Ar atom. In this arrangement, the first Ar atom inside the C4A cavity hinders the interaction between the phenyl rings of C4A and the second Ar atom. We can further estimate the red-shift of {2:0} C4A-Ar_2 by assuming that the red-shift is proportional to the polarizability (ρ) of the guest rare gas atom(s). The polarizability anisotropy ($\Delta\alpha$) of Ar_2 is reported to be 0.3 and 0.5 $Å^3$ by theoretical calculation and experimentally, respectively.[42-44] By using these values we roughly estimate the red-shift of C4A-Ar_2 to be in the range of 53 - 59 cm^{-1}. This value is in good agreement with the observed red-shift of band B (56 cm^{-1}). We checked this assumption from the correlation between the red-shift of various C4A-Rg complexes and the polarizability of the Rg atoms. Upper part of figure 6 shows the plot of the red-shift of the band origin of C4A- Rg_1 against the polarizability of the Rg atom, which is compared with those of benzene- Rg_1 and phenol- Rg_1 complexes. Lower panels of figure 6 show the 2C-R2PI spectra of C4A and various C4A- Rg_1 complexes. A good correlation is seen between the red-shift and the polarizabilities of the Rg atoma and the plot of the observed red-shift of band B vs

the polarizability of Ar_2, which is marked by an asterisk, is in accordance with this relationship. From these results, we conclude that the C4A-Ar_2 complex corresponding to band B, possesses the {2:0} *endo*- structure.

4.5 Larger C4A-Ar_n (n=3-5) complexes

The structures of the larger C4A-Ar_n complexes can be considered to originate from the C4A-Ar_2 {2:0} isomer since their red shifts show a similar trend with that of C4A-Ar_2 as seen in Figure 1(a). This means that the C4A-Ar_n complexes adopt the {n:0} *endo*-isomer structure. The reason that the population of {n:0} *endo*-isomer structure excels over other {m:n-m} isomers is not clear. One of the possibilities is that the collision dynamics in the supersonic jet controls the predominance of *endo*-complex structures. That is the larger size *endo*-isomer complex structure may be formed by the capture of the preformed Ar_n complexes by C4A, instead of the sequential clustering of the Ar atoms with the C4A core. In addition, C4A has a high affinity for encapsulating molecule(s) in its cavity[1-3]. Another possibility is that the *endo-exo* complex has a fast relaxation process in the S_1 electronic state that prevents detection. However, in case of Bz-Ar_2 or Ph-Ar_2, no fast nonradiative process has been reported for the {1:1} isomer compared to the {2:0} isomer at the S_1 zero-point level. Thus, as far as the Ar atoms are bound to the benzene π-ring, the detection efficiency in the S_1-S_0 transition may not be different between the *endo-exo* complex and *endo*-complex at the S_1 zero-point level. Thus, the above reasons reinforce our thesis that the *endo*-isomers are the major species in the supersonic jet and the larger C4A-Ar_n

complexes adopt structures in which Ar_n "snowballs" are bound to the cavity of C4A.

4.6 Additivity of the interaction energies of the C4A-Ar_n (n=1, 2) complexes

The interaction between Ar and the C4A cavity in the *endo*- C4A-Ar isomer can be - to a first approximation – thought of as the sum of the interactions of the Ar atom with the 4 phenyl rings that comprise the C4A cavity. The validity of this approximation is shown in Table 5 where the D_e(*endo*-C4A-Ar) is compared to 4×D_e(Bz-Ar) and 4×D_e(Ph-Ar), i.e it is seen whether it can be constructed in an additive manner from the individual Bz-Ar and Ph-Ar interactions. The average of the uncorrected and BSSE-corrected binding energies (from Tables 2 and 4) are used to test this hypothesis. From Table 5 it can be seen that the MP2/aug-cc-pVDZ results are a bit "erratic" suggesting that there is no additivity in the interactions. However, upon increasing the basis set the predicted 4×D_e values for either Bz-Ar or Ph-Ar come quite close to either the calculated (at the MP2 level) or the estimated [at the CCSD(T) level] value for D_e(*endo*-C4A-Ar). The difference between these 2 numbers, when the interaction energies for Bz-Ar are used, amounts to 67 cm^{-1} (MP2) and 63 cm^{-1} [CCD(T)] for the aug-cc-pVTZ basis set and to -20 cm^{-1} (MP2) and 9 cm^{-1} [CCSD(T)] for the aug-cc-pVQZ set. This suggests that the assumption of the additivity of the various interactions is pretty accurate. This is also the case, albeit to a lesser extend, when the binding energies for Ph-Ar are used. In that case the differences are -37 cm^{-1} (MP2) and -25 cm^{-1} [CCSD(T)] for the aug-cc-pVTZ basis set and -124 cm^{-1} (MP2) and -83 cm^{-1} [CCSD(T)] for the aug-cc-pVQZ basis set. Therefore we can assume that the

total interaction between C4A-Ar can be reproduced to within <1% from the constituent Bz-Ar (<5% from the Ph-Ar) interactions. This error bar is also indicative of the non-additive effects.

As regards the energetics of the C4A-Ar_2 complex we have found that the additivity rule holds better for the {1:1} than for the {2:0} isomer, as one might expect due to the larger 3-body effect for the latter isomer. Indeed, for the {1:1} isomer the interaction can be approximated by:

$$D_e\{1:1\} \approx D_e\,[\text{C4A-Ar};\textit{endo}] + D_e\,[\text{C4A-Ar};\textit{exo}]$$

Using MP2/aug-cc-pVDZ (uncorrected) binding energies, the left part yields 4141 cm^{-1} (3135 + 1066 cm^{-1} from Table 4) whereas the calculated binding energy at that level is 4093 cm^{-1}, just 48 cm^{-1} shy of the predicted one. Similarly, the interaction energy of the {2:0} isomer can be approximated as:

$$D_e\{2:0\} \approx D_e\,[\text{C4A-Ar};\textit{endo}] + D_e\,[\text{Bz-Ar}] + D_e\,[\text{Ar-Ar}],$$

yielding a value of 3814 cm^{-1}, which is 192 cm^{-1} less than the calculated 4006 cm^{-1} binding energy for the {2:0} isomer. The 3-body term should actually be larger than 192 cm^{-1} as the interaction of the second Ar atom with the phenyl ring is much smaller than D_e [Bz-Ar] because the second Ar atom is elevated with respect to the first one inside the cavity. This would yield a less-than-optimal arrangement to interact with the phenyl ring, manifested by the smaller red shift of band B (11 cm^{-1}) with respect to band A as discussed earlier in this section.

5. Conclusions

We have investigated the structures and energetics of the calix[4]arene(C4A)-Ar_n complexes via a joint experimental and theoretical study. For the C4A-Ar complex two isomers were identified: one is the *endo*-isomer (Ar atom lies inside the C4A cavity), which is the major species, and the other is the *exo*-isomer (Ar atom lies outside the C4A cavity). The binding energy of the most stable *endo*-isomer is three times larger than that of the *exo*-isomer. The energetics of these isomers have been determined at the MP2 and CCSD(T) level of theory; the latter represent the current state-of-the-art in the field of large scale, highly correlated electronic structure methods. For the C4A-Ar_2 complex, our calculations predicted two almost isoenergetic isomers, the most stable {2:0} isomer, in which both Ar atoms reside inside the cavity, and the {1:1} isomer, in which one Ar atom is inside and the other outside the cavity. However, the spectral shifts suggested that only the most stable {2:0} isomer is formed. For the larger C4A-Ar_n (n=3-5) complexes, the analysis of their spectral shifts suggests that they also adopt the {n:0} *endo*-structure, that is the Ar_n complex is encapsulated inside the C4A cavity. Though the reason for the predominance of *endo*- complex structures is not clear, the collision dynamics in the expansion region and a high affinity of C4A for encapsulating guest molecule(s) can be given as a possible reason. That is the larger size *endo*-isomer complex structure may be formed by the capture of the preformed Ar_n complexes by C4A, instead of the sequential clustering of the Ar atoms with the C4A core.

Acknowledgments: Part of this work was supported by the Chemical Sciences, Geosciences and Biosciences Division, Office of Basic Energy Sciences, US Department of Energy. Battelle operates the Pacific Northwest National Laboratory for the U.S. Department of Energy. This research was performed in part using the Molecular Science Computing Facility (MSCF) in the Environmental Molecular Sciences Laboratory, a national scientific user facility sponsored by the Department of Energy's Office of Biological and Environmental Research. Additional computer resources were provided at the National Center for Computational Sciences at Oak Ridge National Laboratory, which is supported by the Office of Science of the U.S. Department of Energy under Contract No. DE-AC05-00OR22725. T. E. acknowledges JSPS for the support through a Grant-in-Aid project (No. 18205003) and MEXT for the support through a Grant-in-Aid for the Scientific Research on Priority Area "Molecular Science for Supra Functional Systems" (No. 477).

References

1. C. D. Gutsche, "Calixarenes", in *Monographss in Supramolucular Chemistry*, ed. Stoddart, J. F. Royal Society of Chemistry, Cambridge, **1989.**
2. D. J. Cram, J. M. Cram, "Container molecules and their guests", in *Monographss in Supramolucular Chemistry*, ed. Stoddart, J. F. Royal Society of Chemistry, **1994.**
3. C. D. Gutsche, "Calixarenes revisited", in *Monographss in Supramolucular Chemistry*, ed. Stoddart, J. F. Royal Society of Chemistry, Cambridge, **1998.**

4. K. Araki, K. Iwamoto, S. Shinkai, T. Matsuda, *Bull. Chem. Soc. Jpn.* **1990**, *63*, 3480.
5. I. D. Cunningham, M. Woodfall, *J. Org. Chem.* **2005**, *70* , 9248.
6. F. F. Nachtigall, M. Lazzarottoa, F. Nome, *J. Braz. Chem. Soc.* **2002**, *13*, 295.
7. R. Puchta, T. Clark, W. Bauer, *J. Mol. Model,* **2006**, *12*, 739.
8. F. Benevelli, W. Kolodziejski, K. Wozniak, J. Klinowski, *Chem. Phys. Lett.* **1999**, *308*, 65.
9. M. A.Molins, P. M. Nieto, C. Sanchez, P. Prados, J. De. Mendoza, M. Pons, *J. Org. Chem.* **1992**, 57, 6924.
10. S. Buscemi, A. Pace, A. P. Piccionello, S. Pappalardo, D. Garozo, T. Pilati, G. Gattuso, A. Pappalardo, I. Pisagatti, M. F. Parisi, *Tetrahed. Lett.* **2006**, *47*, 9049.
11. R. Kuzmicz, L. Dobrzycki, K. Wozniak, F. Benevelli, J. Klinowski, W. Kolodziejski, *Phys. Chem. Chem. Phys.* **2002**, *4*, 2387.
12. C. A. Schalley, R. K. Castellano, M. S. Brody, D. M. Rudkevich, G. Siuzdak, J. Jr. Rebek, *J. Am. Chem. Soc.* **1999**, *121*, 4568.
13. R. Zadmard, A. Kraft, T. Schrader, W. Linne, *Chem.-A Europ. J.* **2004**, *10*, 4233.
14. N. Hontama, Y. Inokuchi, T. Ebata, C. Dedonder-Lardeux, C. Jouvet, S. S. Xantheas, *J. Phys. Chem. A* Publication Date (web): August 20, **2009**
15. T. Ebata, Y. Hodono, T. Ito, Y. Inokuchi, *J. Chem. Phys.* **2007**, *126*, 141101.
16. T. Ebata, *Bull. Chem. Soc. Jpn.* **2009**, *82*, 127.
17. C. Møller, M. S.Plesset, *Phys. Rev.* **1934***, 46,* 618.
18. J. Cizek, *J. Chem. Phys.* **1966**, *45*, 4256.

19. R. J. Bartlett, M. Musial, *Rev. Mod. Phys.* **2007**, *79*, 291.

20. T. H. Dunning, *J. Chem. Phys.* **1989***, 90,* 1007.

21. R. A. Kendall, T. H. Dunning, R. J. Harrison, *J. Chem. Phys.* **1992***, 96,* 6796.

22. S. F. Boys, F. Bernardi, *Mol. Phys.* **1970**, *19*, 553.

23. S. S. Xantheas, *J. Chem. Phys.* **1996**, *104*, 8821.

24. T. H. Dunning, *J. Phys. Chem. A* **2000**, *104*, 9062.

25. S. S. Xantheas, T. H. Dunning, *J. Phys. Chem.* **1993**, *97*, 18.

26. H. Koch, B. Fernandez, O. Christiansen, *J. Chem. Phys.* **1998**, *108*, 2784.

27. http://www.emsl.pnl.gov/capabilities/computing/comp_center/chinook_details.jsp

28. E. Bylaska and et al. NWChem, A Computational Chemistry Package for Parallel Computers, Version 5.1, **2007 [Authors names are missing]**

29. V. Tipparaju, E. Aprà, in preparation

30. E. Aprà, R. J. Harrison, W. A. deJong, A. P. Rendell, V. Tipparaju, S. S. Xantheas, *SC'09: Proceedings of the Conference on High Performance Computing, Networking, Storage and Analysis,* SESSION: Gordon Bell finalists, article No. 66, Published by ACM, New York, NY USA (2009). ISBN:978-1-60558-744-8. DOI: http://doi.acm.org/10.1145/1654059.1654127

31. Th. L. Grebner, H. J. Neusser, *Int. J. Mass Spectrom. Ion processes* **1996**, *159,* 137.

32. H. Shinohara, S. Sato, K. Kimura, *J. Phys. Chem. A* **1997**, *101*, 6736.

33. W. Klopper, H. P. Lüthi, Th. Brupbacher, A. Bauder, *J. Chem. Phys.* **1994**, *101*, 9747.

34. R. K. Sampson, W. D. Lawrence, *Austr. J. Chem.* **2003**, *56*, 275.

35. C. E. H. Dessent, S. R. Haines, K. Müller-Dethlefs, *Chem. Phys. Lett.* **1999**, *315*, 103.

36. S.-I. Ischiuchi, M. Sakai, Y. Tsuchida, A. Takeda, Y. Kawashima, M. Fujii, O. Dopfer, K. Müller-Dethlefs, *Ang. Chem. Int. Ed.* **2005**, *44*, 6149.

37. S.-I. Ishiuchi, Y. Tsuchida, O. Dopfer, K. Müller-Dethlefs, M. Fujii, *J. Phys. Chem. A* **2007**, *111*, 7569.

38. T. Weber, A. von Barge, E. Riedle, H. J. Neusser, *J. Chem. Phys*. **1990,** *92*, 90.

39. R.A. Aziz, *J. Chem. Phys.* **1993**, *99*, 4518.

40. M. Schmidt, M. Mons, J. Le Calvé, *Chem. Phys. Lett*. **1991**, *177*, 371.

41. N. Gonohe, H. Abe, N. Mikami, M. Ito, *J. Phys. Chem.* **1985**, *89*, 3642.

42. B. Fernández, C. Háttig, H. Koch, A. Rizzo, *J. Chem. Phys*. **1999**, *110*, 2872.

43. J. Marouli, *J. Phys. Chem. A* **2000**, *104*, 4772.

44. S. Minemoto, H. Tanji, H. Sakai, *J. Chem. Phys.* **2003**, *119*, 7737.

45. Th. Weber, E. Riedle, H. J. Neusser, E. W. Schlag, *Chem. Phys. Let*. **1991**, *183*, 77.

46. M. Mons, J. Le Calvé, F. Piuzzi, I. Dimicoli, *J. Chem. Phys.* **1990**, *92*, 2155.

47. S. Ullrich, G.Tarczay, K. Müller-Dethlefs, *J. Phys. Chem. A* **2002**, *106*, 1496.

Table 1. Frequencies of band origin and red-shift (cm^{-1}) of C4A-Ar_n and C4A-Ne_n.

n	C4A-Ar_n		C4A-Ne_n	
0	35357	-	35357	-
1[a)]	35312	-45	35348	-9
1*[b)]	35297	-60		
2	35301	-56	35345	-12
3	35292	-65		
4	35285	-72		
5	35280	-77		

a) *endo*-compex. b) *exo*-complex.

Table 2. Binding energies (cm^{-1}) of Bz-Ar and Ph-Ar at the MP2 and CCSD(T) levels of theory with the aug-cc-pV*n*Z (*n*=D, T, Q) basis sets. "Average" stands for the average value between the uncorrected and BSSE-corrected binding energies. A harmonic (MP2/aug-cc-pVDZ) estimate of 59.0 cm^{-1} (Bz-Ar) and 59.6 cm^{-1} (Ph-Ar) is used to calculate D_0 from the "Average" values.

Theory	Basis set	D_e (cm^{-1})	D_e (BSSE) (cm^{-1})	"Average" (cm^{-1})	D_0 (cm^{-1})	Exp. (cm^{-1})
			$C_6H_6\cdots Ar$ (Bz-Ar)			
MP2	aug-cc-pVDZ	590	375	482	423	
	aug-cc-pVTZ	669	506	587	528	
	aug-cc-pVQZ	623	551	587	528	
CCSD(T)	aug-cc-pVDZ	426	197	311	252	
	aug-cc-pVTZ	480	319	400	341	
	aug-cc-pVQZ	419	358	388	329	**314±7** [a]
			$C_6H_5OH\cdots Ar$ (Ph-Ar)			
MP2	aug-cc-pVDZ	658	395	527	467	
	aug-cc-pVTZ	698	528	613	553	
	aug-cc-pVQZ	652	574	613	553	
CCSD(T)	aug-cc-pVDZ	494	215	354	294	
	aug-cc-pVTZ	506	339	422	362	
	aug-cc-pVQZ	443	378	411	351	**359** [b]

[a] Ref. 34

[b] Ref. 36

Table 3. CCSD(T) binding energies (D_e) as a percentage of the corresponding MP2 ones for the Bz-Ar and Ph-Ar complexes for the various basis sets.

Basis set	% MP2 (uncorr.)	% MP2 (BSSE)	% MP2 "Average"
	C_6H_6···Ar (Bz-Ar)		
aug-cc-pVDZ	72.2	52.5	64.5
aug-cc-pVTZ	71.7	63.1	68.1
aug-cc-pVQZ	67.1	65.0	66.1
	C_6H_5OH···Ar (Ph-Ar)		
aug-cc-pVDZ	75.1	54.3	67.2
aug-cc-pVTZ	72.5	64.1	68.8
aug-cc-pVQZ	68.0	65.8	67.0

Table 4. Calculated and predicted (italics in parentheses) binding energy of the "inside" and "outside" isomers of C4A-Ar. The predicted values for D_e at the CCSD(T) level of theory are obtained from the corresponding MP2 values and CCSD(T)/MP2 ratios from the Ph-Ar system.

Theory	Basis set	D_e (cm^{-1})	D_e (BSSE) (cm^{-1})	"Average" (cm^{-1})	Exp. (cm^{-1})
		C4A-Ar (*endo* isomer)			
MP2	aug-cc-pVDZ	3135	1733	2434	
	aug-cc-pVTZ	2720	2111	2415	
	aug-cc-pVQZ	2440	2217	2328	
CCSD(T)	aug-cc-pVDZ	2467	1013	1740	
		(*2355*)	(*940*)	(*1635*)	
	aug-cc-pVTZ	(*1972*)	(*1353*)	(*1663*)	
	aug-cc-pVQZ	(*1659*)	(*1460*)	(*1561*)	350 – 2250 [a]
		C4A-Ar (*exo* isomer)			
MP2	aug-cc-pVDZ	1066	513	790	
	aug-cc-pVTZ	942	717	830	
	aug-cc-pVQZ	817	707	762	
CCSD(T)	aug-cc-pVDZ	(801)	(279)	(530)	
	aug-cc-pVTZ	(683)	(460)	(571)	
	aug-cc-pVQZ	(555)	(465)	(511)	

[a] This study (D_0).

Table 5. Additivity of the phenyl-Ar interaction in the *endo*-isomer of the C4A-Ar complex. D_e corresponds to the average of the uncorrected and BSSE-corrected binding energies (see Tables 2 and 4).

Theory	Basis set	D_e[C4A-Ar] (cm^{-1})	D_e[C4A-Ar]-4×D_e[Bz-Ar] (cm^{-1})	D_e[C4A-Ar]-4×D_e[Ph-Ar] (cm^{-1})
MP2	aug-cc-pVDZ	2434	506	326
	aug-cc-pVTZ	2415	67	-37
	aug-cc-pVQZ	2328	-20	-124
CCSD(T)	aug-cc-pVDZ	1740	496	324
	aug-cc-pVTZ	1663	63	-25
	aug-cc-pVQZ	1561	9	-83

Figure captions

Figure 1 Left panel: (a) the LIF spectra of C4A at various Ar partial pressures, and the 2C-R2PI spectra with the monitored masses for (b) $[C4A]^+$ and (c) $[C4A\text{-}Ar_1]^+$. Right panel: time-of-flight spectra of bands A, B and A'.

Figure 2 Left panel: Mass-resolved 2C-R2PI spectra of bare C4A and the C4A-Ar complex via the zero-point level of the S_1 state. Right panel: energy level diagram used to determine the ionization potential and the binding energy.

Figure 3 LIF spectra of (a) C4A, (b) C4A-d_n and (c) C4A-d_n-Ar. (d) Fragment detected IR photodissoication (FDIRPD) spectrum of C4A-d_0-Ar complex. (e) (upper) Fragment detected IR photodissoication (FDIRPD) spectrum of the mixture of C4A-$d_{1,2,3}$-Ar complexes. (lower) Simulated IR spectrum of the mixture of C4A-$d_{1,2,3}$-Ar complexes. For the details, see the text.

Figure 4 Optimized structures of (a) C4A-Ar_1 *endo*-complex and (b) C4A-Ar_1 *exo*-complex and their top and side views.

Figure 5 Optimized structures of (a) C4A-Ar_2 {2:0} complex and (b) C4A-Ar_2{1:1} complex, and their top and side views.

Figure 6 (upper) Plot of the red-shift of the band origin of C4A-Rg_1 against the polraizability of Rg-atom. An asterisk coppesponds to C4A-Ar_2. Also shown are those of benzene-Rg_1 and phenol-Rg_1 complexes. (lower) Mass-selected 2C-R2PI spectra of the C4A-Rg_1 ccomplexes. The red-shifts of benzene-Rg_1 and phenol-Rg_1 complexes are adopted from Refs. 45-47.

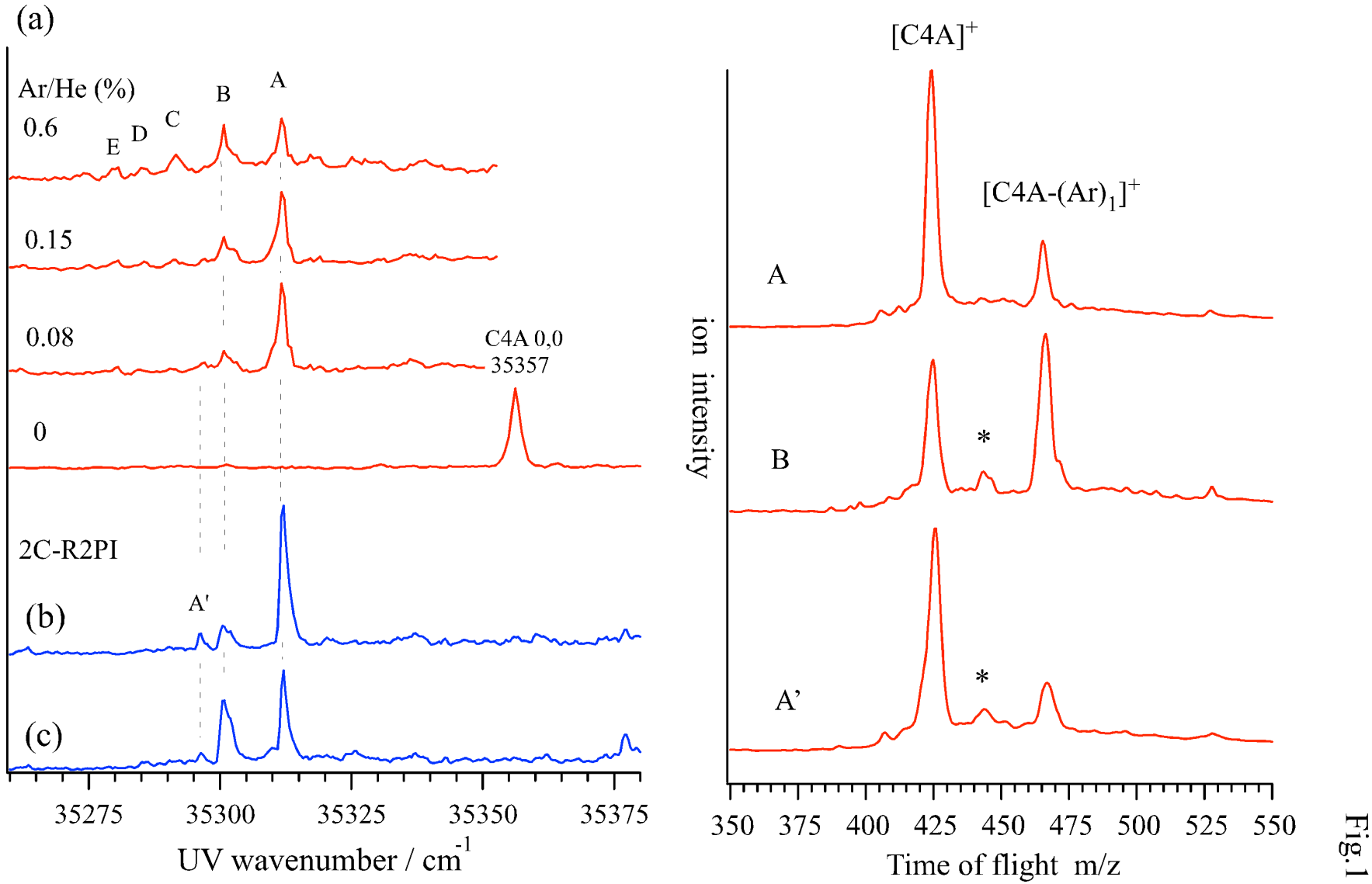
(a)
Ar/He (%)
0.6
0.15
0.08
0
E
D
C
B
A
C4A 0,0
35357
2C-R2PI
(b)
(c)
A'
35275
35300
35325
35350
35375
UV wavenumber / cm-1
[C4A]+
[C4A-(Ar)1]+
A
B
A'
*
*
ion intensity
350
375
400
425
450
475
500
525
550
Time of flight m/z

Fig.1

Fig. 2

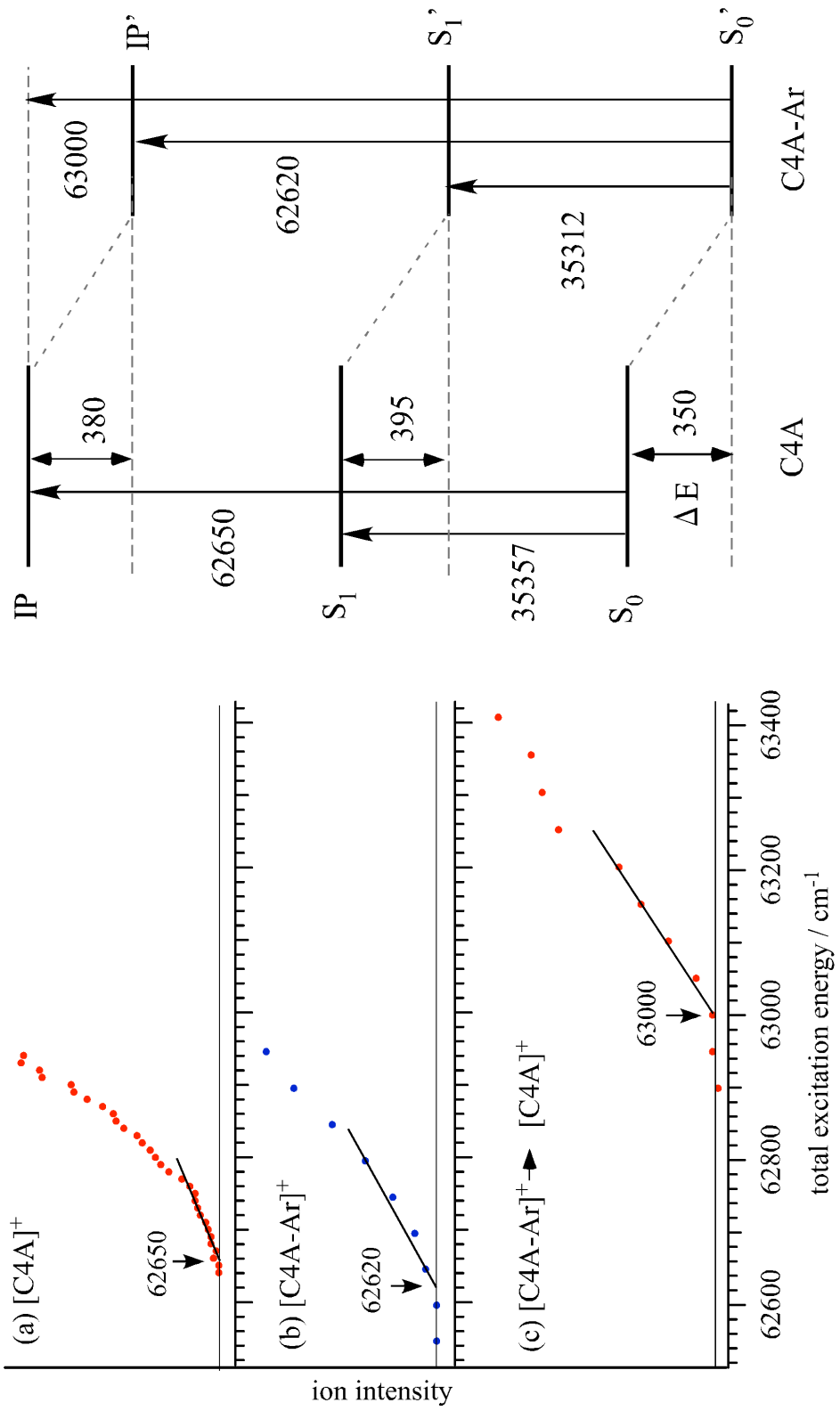
IP
IP'
S1
S1'
S0
S0'
63000
62620
62650
380
395
350
35312
35357
ΔE
C4A
C4A-Ar
(a) [C4A]+
(b) [C4A-Ar]+
(c) [C4A-Ar]+ → [C4A]+
62650
62620
63000
ion intensity
62600
62800
63000
63200
63400
total excitation energy / cm-1

Fig. 3

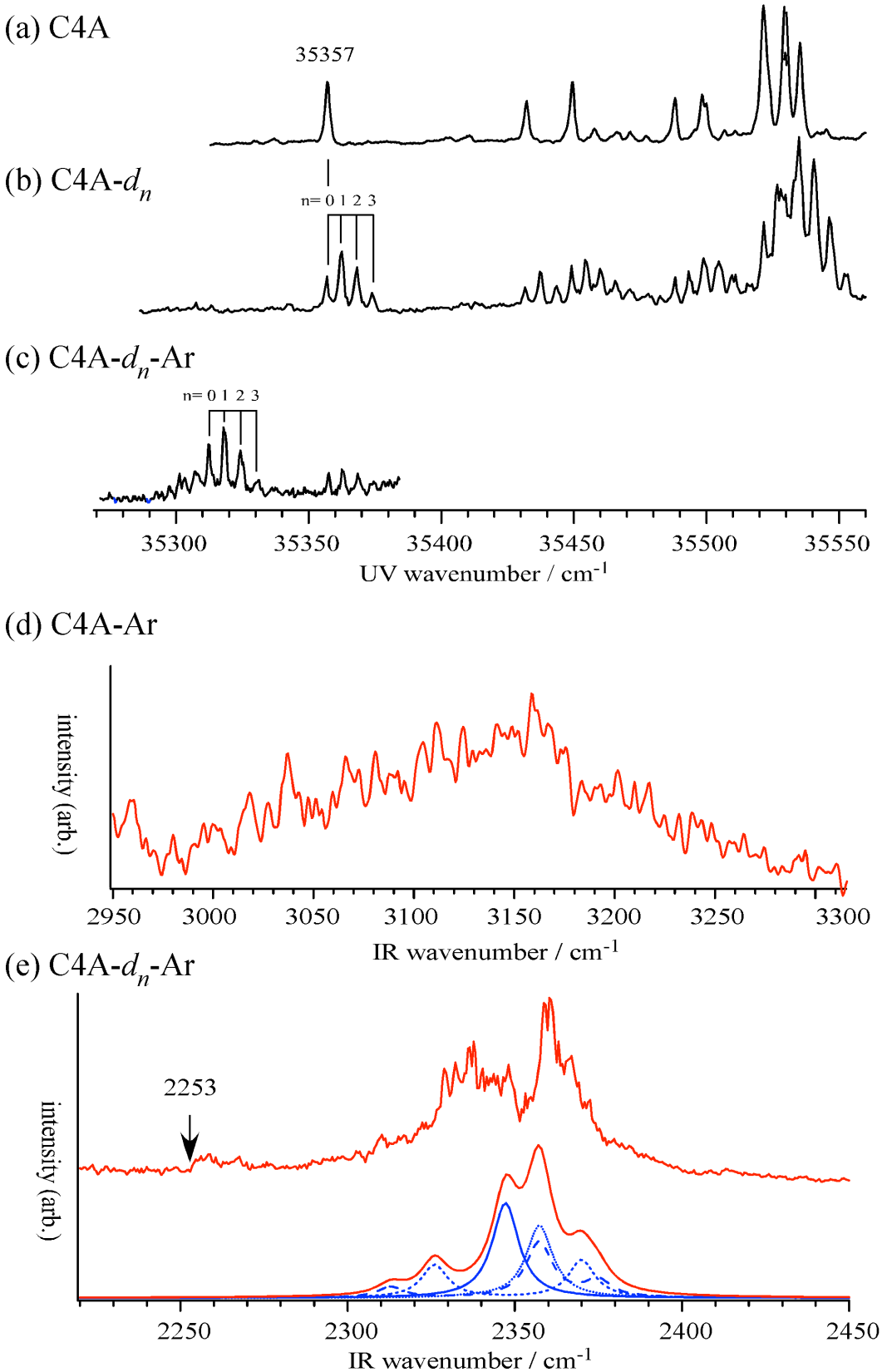
(a) C4A
35357
(b) C4A-d_n
n= 0 1 2 3
(c) C4A-d_n-Ar
n= 0 1 2 3
35300
35350
35400
35450
35500
35550
UV wavenumber / cm^{-1}
(d) C4A-Ar
intensity (arb.)
2950
3000
3050
3100
3150
3200
3250
3300
IR wavenumber / cm^{-1}
(e) C4A-d_n-Ar
2253
intensity (arb.)
2250
2300
2350
2400
2450
IR wavenumber / cm^{-1}

Fig. 4

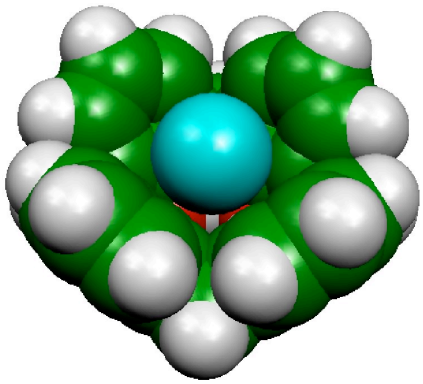

(a) C4A-Ar *endo*-complex

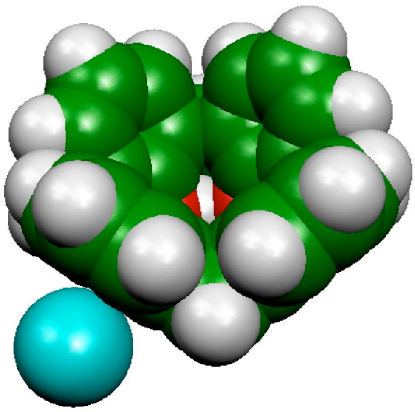

(b) C4A-Ar *exo*-complex

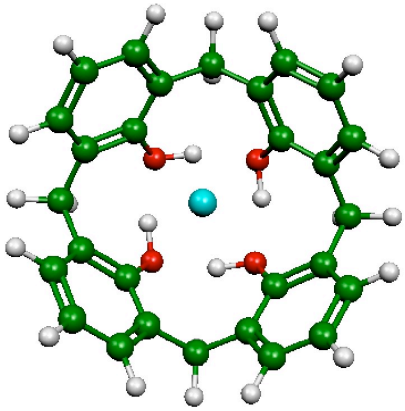

top view

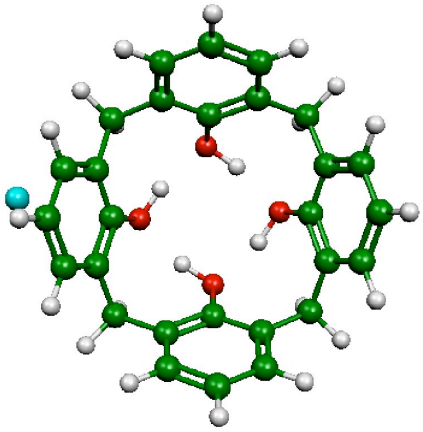

top view

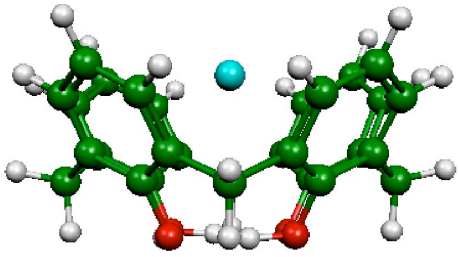

side view

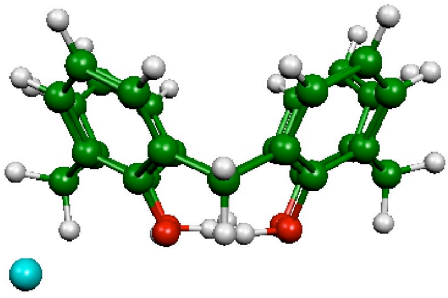

side view

Fig. 5

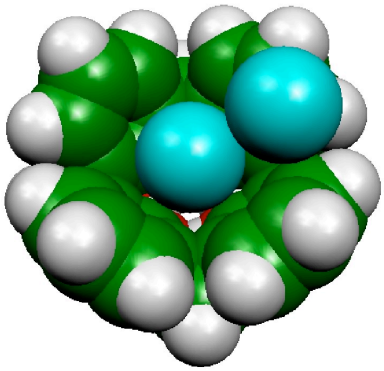

(a) C4A-Ar_2 {2:0}complex

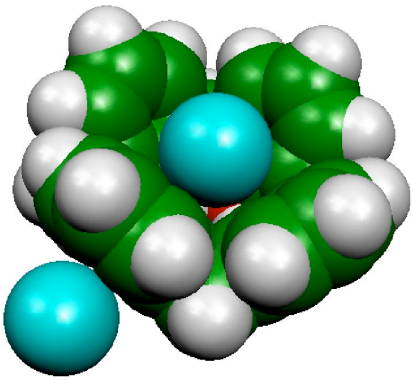

(b) C4A-Ar_2 {1:1}complex

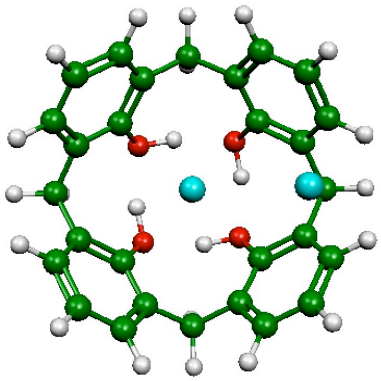

top view

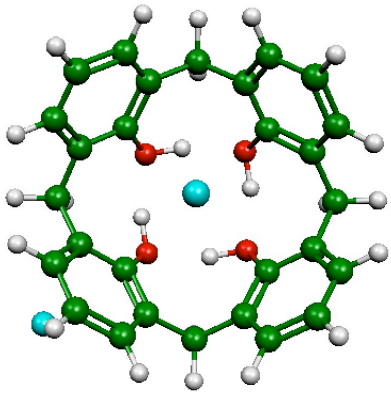

top view

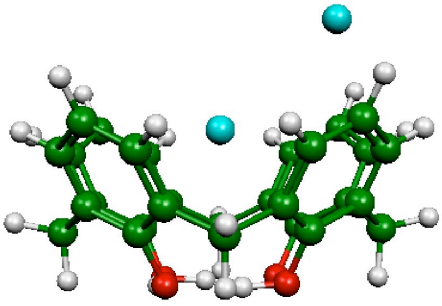

side view

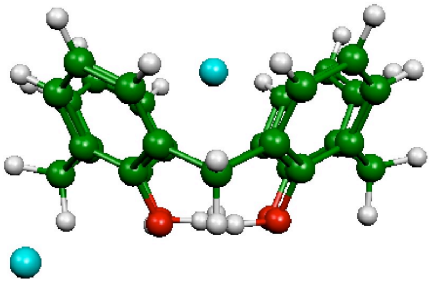

side view

Fig. 6

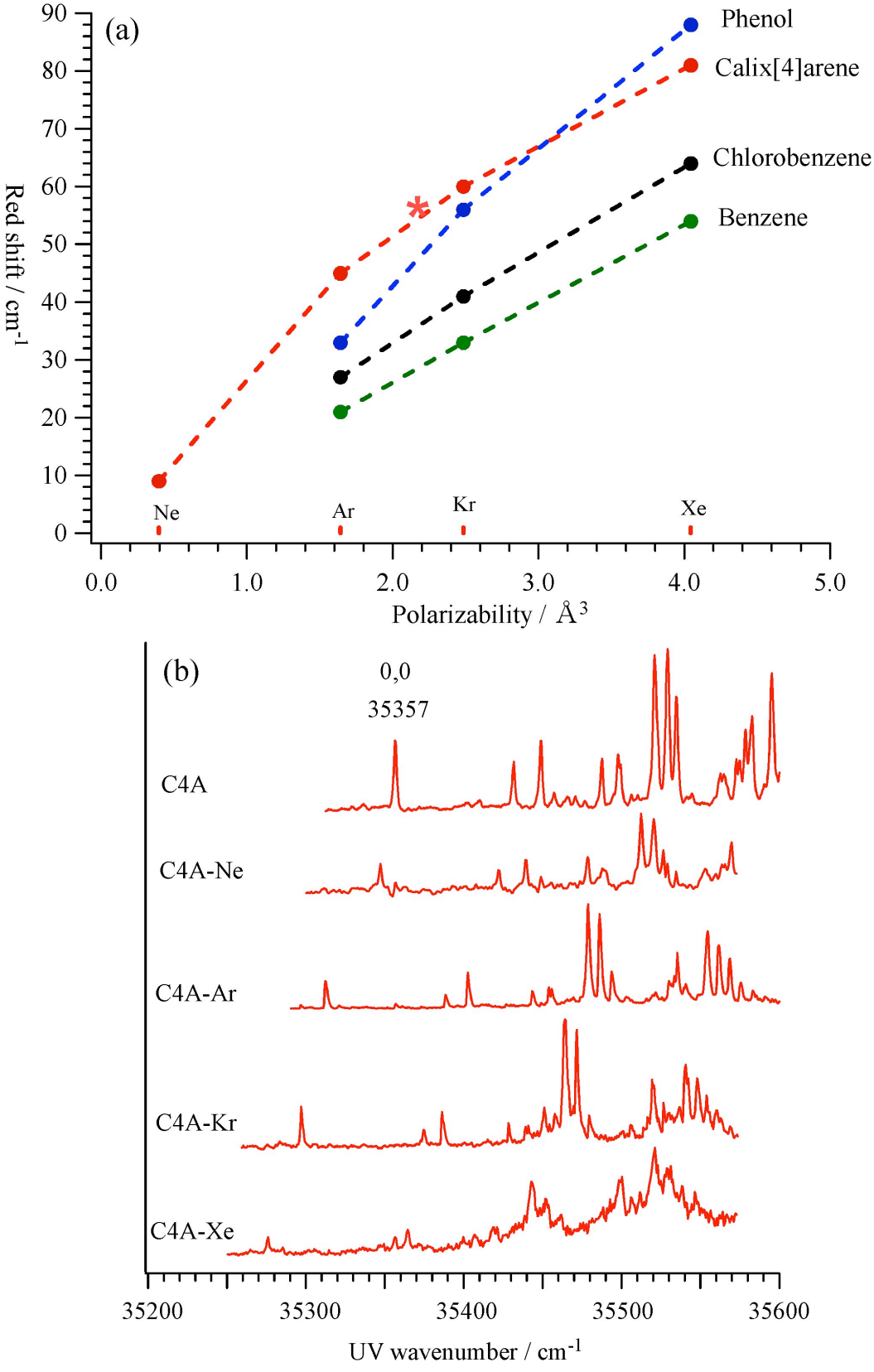
(a)
Red shift / cm-1
Polarizability / Å3
Phenol
Calix[4]arene
Chlorobenzene
Benzene
Ne
Ar
Kr
Xe
(b)
0,0
35357
C4A
C4A-Ne
C4A-Ar
C4A-Kr
C4A-Xe
UV wavenumber / cm-1